The method used here does not assume independence between successive recoils of the hole; that assumption does seem to appear in the methods of Müller-Hartmann *et al.*[13] and of Doniach.[5]

*Research sponsored by the Air Force Office of Scientific Research under Contract No. AF 49 (638)-1545.

†Present address: Theoretical Physics Department, The Hebrew University, Jerusalem, Israel.

‡Work performed in part at Battelle Memorial Institute, Columbus, Ohio.

[1]G. D. Mahan, Phys. Rev. 163, 612 (1967).

[2]P. Nozières and C. T. De Dominicis, Phys. Rev. 178, 1084 (1969).

[3]K. D. Schotte and U. Schotte, Phys. Rev. 182, 479 (1969).

[4]S. Doniach, Phys. Rev. B 2, 3898 (1970).

[5]S. Doniach and M. Sunjic, J. Phys. C 3, 285 (1970).

[6]J. Gavoret, P. Nozières, B. Roulet, and M. Combescote, J. Phys. (Paris) 30, 987 (1969).

[7]S. Tomonaga, Progr. Theoret. Phys. (Kyoto) 5, 544 (1950).

[8]R. P. Feynman, Ph. D. thesis (Princeton University, 1942) (unpublished); Phys. Rev. 84, 108 (1951).

[9]See R. P. Feynman and A. R. Hibbs, *Quantum Mechanics and Path Integrals* (McGraw-Hill, New York, 1965), Eq. (8-138), for the derivation of this for one oscillator.

[10]We write $1/(1+t^2) - \pi\delta(t)$, instead of just $1/t^2$, in order to get the correct Fourier coefficients at zero frequency ($E=0$).

[11]Which, among other things, means neglecting the finite hole lifetime due to the creation of electron-hole pairs.

[12]A $[(\sin^2 kr)/r^2]$ potential always has bound states (like those of an inverse-square potential) but these become very weakly bound for a weak potential, and need not concern us.

[13]E. Müller-Hartmann, T. V. Ramakrishnan, and G. Toulouse, Phys. Rev. B 3, 1102 (1971).

PHYSICAL REVIEW B VOLUME 4, NUMBER 12 15 DECEMBER 1971

Photoemission Studies of Indium†

R. Y. Koyama* and W. E. Spicer
Stanford University, Stanford, California 94305

(Received 28 June 1971)

Measurements of the electron energy distributions of photoemitted electrons from crystalline and bulk liquid samples of indium show structure which can be related to the occupied density of states. The distributions from the crystalline sample show two major peaks: a strong one just below the Fermi level and a weaker one about 4.5 eV below the Fermi level. Similar structure in the distributions from the liquid sample suggest that electron energy levels for indium are determined primarily from short-range interactions. Two model calculations based on direct transitions and nondirect transitions can each predict the observed structure with reasonable accuracy. In either calculation, structure in the energy distributions can be traced to similar structure in the density of valence states.

I. INTRODUCTION

The initial motivation of this work was to investigate the importance of long-range order in a nearly free-electron metal by studying photoemission from crystalline and amorphous indium. Although we did not anticipate it at the onset of the work, it has become evident that the photoemission from crystalline indium is itself not unambiguously explained in terms of a single simple model. Rather, it has proved necessary to investigate direct[1] and nondirect[2] optical excitation models and to consider the possibility of surface excitation of plasmon effects.[3] However, it appears that independent of the detailed model, it is possible to associate structure in the photoemission energy distribution curves (EDC) from crystalline indium with structure in the density of states. This allows for rather direct comparison between the photoemission results from crystalline and liquid indium.

As one might expect, we find that indium has an electronic structure that is relatively free-electron-like. Its optical properties[4] are quite similar to those of aluminum. The measurements we present here indicate that the energy bands of indium are distorted somewhat more than those of aluminum from the "pure" free-electron case. Structure in the electron energy distributions suggest stronger interaction of the electron with the lattice potential.

II. EXPERIMENTAL METHODS

A. Measurements

The two experimental quantities of interest are the quantum yield and the photoelectron energy distribution. The quantum yield is defined as the

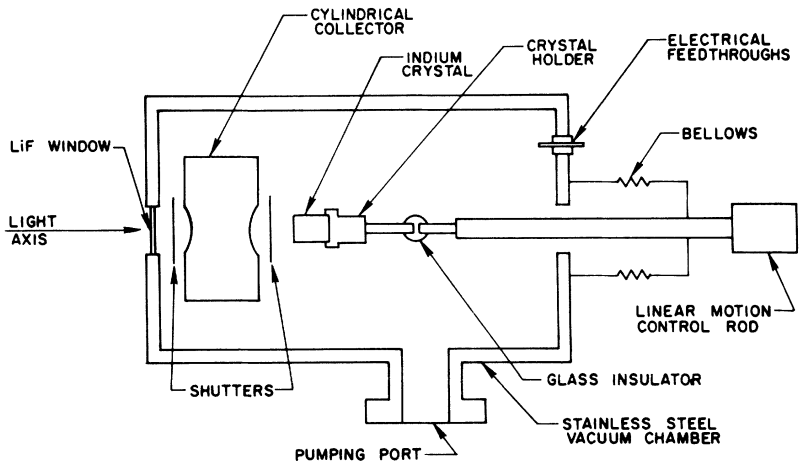

FIG. 1. Schematic diagram of the apparatus used to measure the photoemission properties of crystalline indium.

total number of photoemitted electrons per absorbed photon; this quantity is measured by collecting all emitted electrons and referring them to the incident photon flux. Corrections are made for reflection losses at the surface. The absolute incident photon flux was determined by using a calibrated Cs_3Sb cell as a reference standard.[5] The energy distribution of electrons was measured with a cylindrical analyzer using the "ac retarding potential" method.[6] The light source was a 1-m normal-incidence monochromator with a hydrogen Hinteregger lamp. Additional experimental details are given in Ref. 5.

B. Sample Preparation: Crystalline Indium

Photoemission measurements on crystalline samples of indium were made in a small-volume (~2 liter) stainless-steel chamber pumped by an 8-liter/sec ion pump and a titanium getter pump. Mild baking (up to 135 °C to avoid sample destruction) routinely achieved pressures of 5×10^{-9} Torr. A schematic drawing of the vacuum chamber with its sample manipulator is shown in Fig. 1.[7] The LiF window isolates the sample chamber from the monochromator (corrections on the incident flux are made using the measured transmission of the window); the window limits the maximum photon energy to about 11.7 eV. After achieving base pressures in the chamber, a small amount of gold is evaporated inside the collector-analyzer (with the shutter closed) to provide a uniform collector work function. Measurements are made by opening the shutters and inserting the sample into the collector-analyzer.

The indium sample was cut from a "single-crystal" rod of 99.99 at.% purity using a spark saw. The planar, but textured, surface was briefly etched in a solution of HCl acid in methanol (1:2); the etching process revealed grain boundaries, and a typical sample had a large central crystal with several smaller ones surrounding it. X-ray diffraction measurements[8] indicated that the (111) face of the crystal was within 6° of the front surface (the surface was perpendicular to the axis of the rod).

The final cleaning process of the crystalline surface consisted of argon-ion bombardment (10-μ pressure) with the sample withdrawn from the collector-analyzer. The electron energy distribution curve was monitored as a function of bombardment time. In general, the EDC from the uncleaned surface is dominated by a large group of low-energy electrons from the unprocessed sample. These EDC are believed to be due to the contaminated surface of the sample (i.e., oxides and adsorbed gases), as well as the bulk indium.[9] As the bombardment proceeds, contaminants are desorbed from the surface, and higher-energy electrons characteristic of the bulk begin to dominate the EDC. During the cleaning process, the total yield of the sample (at the monitored photon energy 10.2 eV) decreases about an order of magnitude and the work function increases.[5]

A valid point of criticism or question would be that of the effect of ion bombardment on the sample surface. The effect of ion bombardment on the reflectance has been seen on indium surfaces.[4,5] It was found that, as a function of bombardment time, the reflectance increased to some maximum value; subsequently, excessive bombardment caused a degradation of the reflectance. Parallel effects on the EDC were observed. In particular, excessive bombardment caused the number of low-energy electrons to increase relative to the number of high-energy electrons, with the total yield remaining fixed. This would suggest some irreversible damage to the surface, which caused more than ordinary electron scattering at the surface. Similar irreversible effects have also been observed in the optical constants of argon-ion bombarded samples of silver.[10] In the present experi-

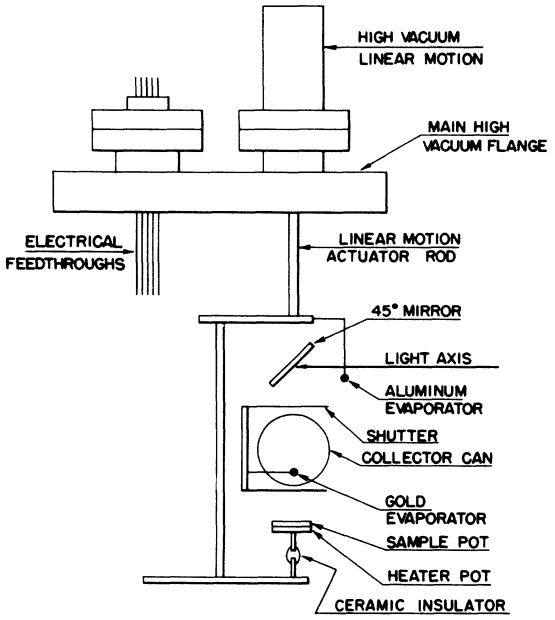

FIG. 2. Schematic diagram of the high-vacuum flange used in the photoemission measurement from liquid indium.

ments, no attempt was made to measure the physical "damage" to the surface. However, the "optimum point" in the cleaning process is that at which the reflectance shows a maximum and the photoemission spectrum shows the highest ratio of high-energy electrons to scattered electrons. Undoubtedly, at this point, a compromise between cleanliness and surface damage is being made. Although we recognize that x rays penetrate deeper into the sample than the probing photon (~10 eV), the diffraction measurements indicated crystallinity of the sample before and after the ion-bombardment process.

C. Sample Preparation: Liquid Indium

Measurements on liquid samples of indium were made in two different experimental systems: One was a sealed-off glass phototube, and the other was an all stainless-steel high-vacuum chamber.[5] Although the data from the two systems were similar, the high-vacuum chamber had distinct advantages including the facility to clean the sample at better vacuums and higher temperatures. For this reason, only the data from the chamber are discussed here.

Figure 2 shows a schematic diagram of the high-vacuum flange which was used for the preparation of the liquid sample and the photoemission measurements. The flange is housed in a stainless-steel chamber with a LiF window on the optical axis. The chamber was pumped by a combination ion and getter pump[11] and routinely achieved base pressures of 6×10^{-11} Torr after a 200 °C bake. A 45° aluminum mirror was used to direct the light beam onto the sample. The energy analyzer is similar to the one mentioned previously, but oriented with the light axis vertical.

Shortly before sealing the flange to the vacuum chamber, the sample pot was loaded with chips or pellets of 99.99 at.% indium. To avoid condensation of contaminants on the sample during the bake cycle, the sample was heated (with the analyzer shutter closed) and maintained at a temperature slightly higher than its surroundings. In addition, the gold and aluminum evaporators were thoroughly outgassed. After reaching base pressures, a layer of gold was evaporated inside the collector-analyzer to provide a uniform collector work function; the aluminum was evaporated onto the glass substrate to form a "fresh" mirror. Final sample preparation involved heating the indium sample to about 800 °C for a short period to evaporate or dissolve any surface impurities. The final-sample surface had a highly specular finish with the sample molten. The frozen solid had a slightly wrinkled finish.

In these experiments, measurements of both liquid and frozen indium were made on the same bulk sample. Room-temperature measurements were made on the frozen solid, whereas those on the liquid were made as the sample cooled from 200 to 185 °C (melting point at 156 °C). X-ray diffraction measurements[8] on the frozen solid showed no signs of crystallinity. Undoubtedly, such noncrystallinity would be expected of the liquid sample. The fact that the frozen sample was noncrystalline suggests that it is disordered like the liquid, i.e., that it is amorphous.

III. EXPERIMENTAL RESULTS

Figure 3 is a family of electron energy distributions for the crystalline sample of indium. The ordinate gives the absolute differential yield (electrons per absorbed photon per eV); the Fermi energy is taken as the zero of energy. Up to photon energies of 9.0 eV, the EDC are characterized by a single broad peak of electrons. As $\hbar\omega$ increases, this peak moves to higher energy by an amount equal to the change in photon energy. At higher photon energies, a low-energy shoulder develops about 4.5 eV below the Fermi energy, and the total yield continues to increase. Near 11.0 eV, the low-energy shoulder becomes discernible as a peak as it just evolves from the strong influence of the threshold. At the highest photon energies, the total yield begins to decrease as evidenced by the decreasing area under the EDC. A property which is characteristic of the photoemission from indium is shown in Fig. 4. Plotted here is a subset of the EDC of

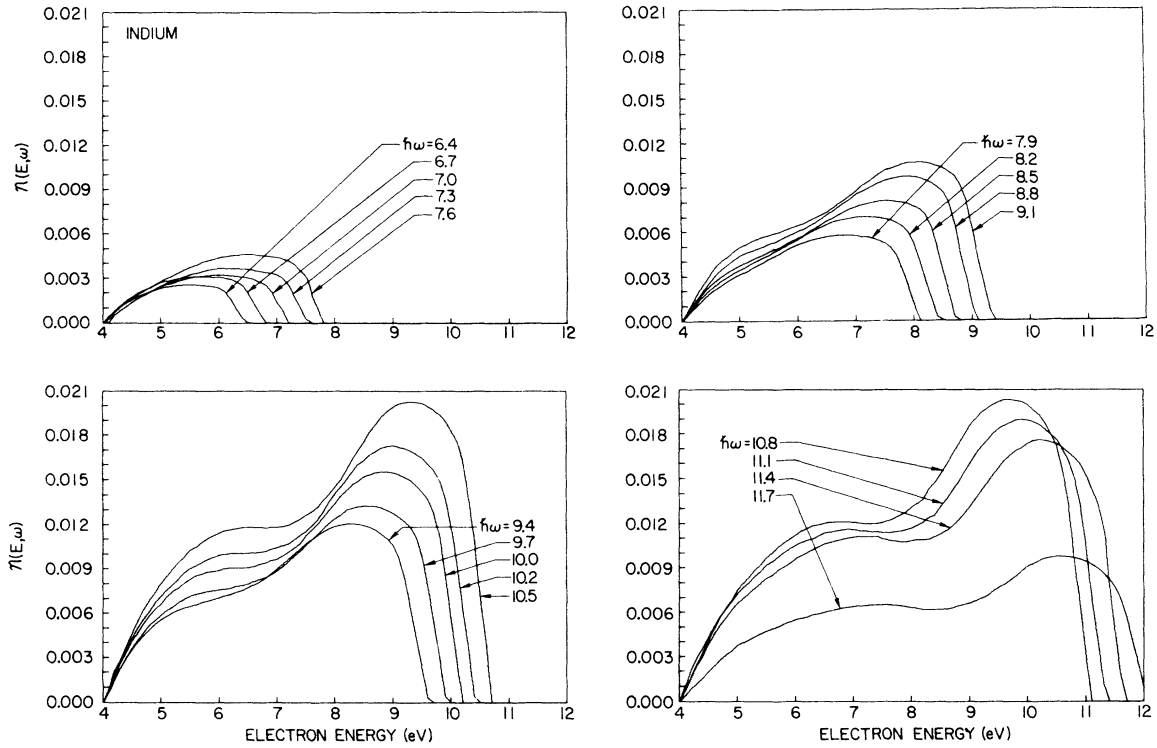

FIG. 3. Normalized electron energy distributions for a sample of crystalline indium.

Fig. 3, with the electron energies referred to their initial states (the Fermi energy is still taken as the zero of energy). We see that the leading peak (near -1.0 eV) and the lower-energy peak (near -4.0 eV) are aligned at the same electron energy for the various photon energies. We believe that both peaks are features which arise from structure in the density of filled states of indium. The reasons for this will become apparent in later sections of this paper.

Figure 5 is a corresponding family of EDC for liquid indium (these are scaled arbitrarily). As we saw in the crystalline sample, the leading peak in these energy distributions moves by an amount equal to the increase in photon energy. There is also a low-energy feature with a character which is somewhat different from that of the corresponding peak in the crystal solid. Namely, it develops into a well-defined peak and grows in intensity relative to the leading high-energy peak. A general character of scattered electrons is to produce a peak at electron energies just above threshold. This peak increases in magnitude but does not increase in energy with increasing photon energy.[9] The low-energy group of Fig. 5 does increase in intensity with increasing photon energy; however, they do not remain fixed in energy with respect to the threshold. They have a finite motion to higher energy with increasing $\hbar\omega$, which eventually moves them away from the threshold. However, the rate of motion is less than the rate of increase in $\hbar\omega$. As mentioned above, such behavior is distinct from usual behavior of scattered electrons which remain at low energy near threshold. This would suggest that the low-energy group is a combination of excitation from a maximum in the valence density of states and a contribution from scattered electrons. This result might also be deduced from the rather significant degradation of the leading high-energy peak with photon energy. These high-energy electrons are rapidly being removed from the primary spectrum by inelastic scattering events. This scattering is not temperature dependent since the room-temperature EDC from the frozen solid displayed virtually the same characteristics. In our measurements, we noted a reversible change of the photoemission threshold with temperature, but little change of the EDC over a range of approximately 200–25 °C (melting point at 156 °C). This might suggest a source of scattering such as a foreign surface layer which was not removed by the cleaning process.

Figure 6 displays the quantum yield for the crystalline sample, the liquid sample, and the solid formed by cooling from liquid. X-ray studies showed the latter to be noncrystalline, i.e., amor-

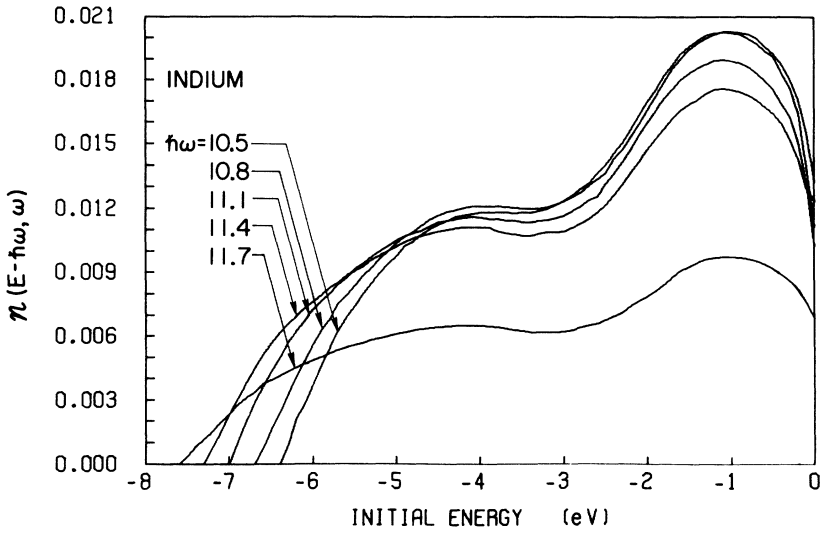

FIG. 4. Partial set of normalized EDC plotted with respect to the initial states.

phous. Corrections for reflection losses on the crystalline sample was made using reflectance data from a similarly prepared optical sample in a high-vacuum reflectometer.[4] The yield data of the liquid and frozen (noncrystalline) solid were corrected using the data of Wilson and Rice.[12] No *in situ* reflectance measurements of photoemission samples were made; therefore, the yield curves of Fig. 6 represent an upper limit. The liquid sample had a specular surface whereas both the frozen solid and the crystal sample had some visible imperfections (i.e., wrinkles on the frozen solid and grain boundaries on the crystal).

By fitting to Fowler plots, work functions were obtained from the three yield curves near threshold. Interestingly, the work functions were found to be identical (4.14±0.05 eV) within experimental error. van Laar and Scheer[13] have reported a work function of 4.08±0.01 eV for evaporated films.

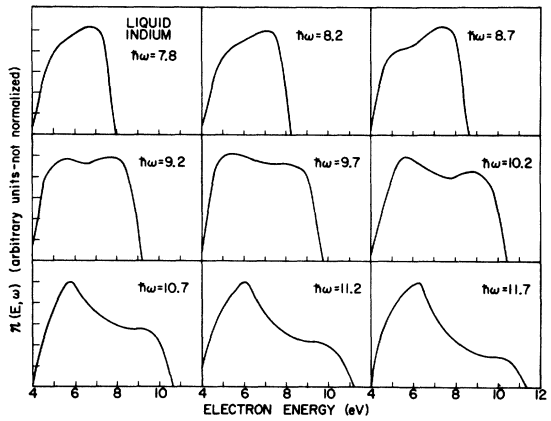

FIG. 5. EDC for a sample of liquid indium (not normalized).

Within a few eV of threshold the magnitude of the yield decreases almost a factor of two when the liquid is cooled to form the room-temperature solid. This change in yield is quite reproducible as the temperature is cycled from room temperature to above the melting point. However, despite the change in magnitude of yield near threshold, the work function obtained from the Fowler plot does not change.

IV. DISCUSSION RESULTS FROM CRYSTALLINE INDIUM

A. Introduction

Spicer[14] and Doniach[15] have given some argu-

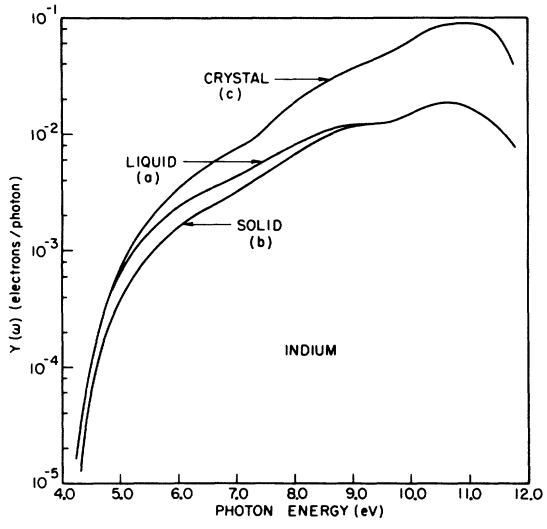

FIG. 6. Measured yields for (a) the liquid sample, (b) the noncrystalline solid sample formed by cooling the liquid, and (c) the crystalline sample.

ments for the validity of the nondirect transition in certain materials. Localization of an excited hole has been suggested as a possible mechanism that will allow a nonvertical transition and a breakdown of $\vec{k}$ conservation. Indium, however, is a relatively free-electron metal with a wide occupied band (8.6 eV). Therefore, there is no *a priori* reason to overlook the direct transition in favor of the nondirect transition. The characteristic feature of stationary structure on an $E-\hbar\omega$ plot (e.g., Fig. 4) is one definite property of nondirect transitions; however, it has been found in certain cases to occur for calculated electron-energy spectra based on direct transitions.[1,16-18] Therefore, this aspect is not exclusive to nondirect transitions. Calculations on aluminum,[1] the noble metals,[16] and palladium[17] show that, despite the necessity to conserve $\vec{k}$, the EDC show some stationary behavior when plotted with respect to $E-\hbar\omega$. Of these metals, aluminum is the most free-electron-like and has no sharp features in the experimental spectrum[19]; the calculated spectra for direct transitions[1] appear to reproduce the density of states in the manner expected of nondirect transitions.

B. EDC Calculated on the Basis of Direct Transitions

We have calculated electron energy distributions for indium as a function of the incident photon energy. The method used to determine the spectra is essentially identical to the method described in Ref. 1; the eigenvalue calculation differs for indium and so will be described here. The indium crystal is a body-centered-tetragonal crystal, and for our convenience, by a 45° rotation about its c axis, we can consider it to be face-centered tetragonal. In this configuration, it has fcc structure, but distorted by 8% along the c axis (for the purposes of discussion, all references to symmetry points will be based on this fct-fcc structure). For fcc aluminum, a $\frac{1}{48}$ symmetry sector of the Brillouin zone was considered, and a calculation using four orthogonalized plane waves (4 OPW) was sufficient[1]; due to the tetragonal distortion in indium, a $\frac{1}{16}$ symmetry sector is required and a minimum of 6 OPW must be used. In order to reduce the computation time, a simplification was made: The $\frac{1}{16}$ sector was divided into three inequivalent parts, each of which corresponded roughly to $\frac{1}{48}$ of the original full Brillouin zone. In each "$\frac{1}{48}$" sector, the appropriate 4-OPW equation (instead of the 6-OPW) was solved. This simplification results in a slight mismatch of energy bands at the two interior contact faces of the three "$\frac{1}{48}$" sectors. However, the number of such mismatched points is small compared to the total number of points and its effect on the results is small. The final result is then calculated as an average of the three sectors. In each sector, an equation of the following type was solved:

$$0=\begin{vmatrix} T_1(\vec{k})-E_i(\vec{k}) & V_{111} & V_{111} & V_{200} \\ V_{111} & T_2(\vec{k})-E_i(\vec{k}) & V_{002} & V_{111} \\ V_{111} & V_{002} & T_3(\vec{k})-E_i(\vec{k}) & V_{111} \\ V_{200} & V_{111} & V_{111} & T_4(\vec{k})-E_i(\vec{k}) \end{vmatrix}, \tag{1}$$

where

$$T_1(\vec{k})=\vec{k}^2, \quad T_2(\vec{k})=(\vec{k}-\vec{K}_{111})^2, \quad T_3(\vec{k})=(\vec{k}-\vec{K}_{111})^2, \quad T_4(\vec{k})=(\vec{k}-\vec{K}_{200})^2. \tag{2}$$

$E_i(\vec{k})$ are the eigenvalues for the energy bands; the $V_{\vec{K}}$ are the Fourier coefficients of the potential arising from the $\vec{K}$th lattice wave vector. These were determined according to a method provided by Ashcroft and Lawrence[20]; they calculated the appropriate potential for a "best fit" to Fermi-surface data. In each sector, Eq. (1) (with the appropriate matrix elements) was solved by reducing the quartic approximately 3×10^5 times giving a total of about 3.5×10^6 contributing eigenvalues. Each point of the $\vec{k}$-space mesh was weighted according to its symmetry in the zone.

The density of states resulting from this calculation is shown in Fig. 7 (dotted curve; the dashed curve will be discussed in Sec. IV C). Up to about 4.0 eV, it rises free-electron-like; above this, three pieces of structure are prominent. Deviation of this density of states from a free-electron behavior is due to the band gaps at the zone boundaries caused by the potential. In an earlier paper, Ashcroft and Lawrence[20] discuss a pseudopotential band-structure calculation for indium. From the potential matrix elements, they determined the band gaps at the various faces of the Brillouin zone of indium. These were then used to calculate the band density of states using the following equation (see also Ref. 21):

$$D(E)\propto\int_{Bz} dQ(E)/\nabla_{\vec{k}}E, \tag{3}$$

where Bz means Brillouin zone and $dQ(E)$ is an

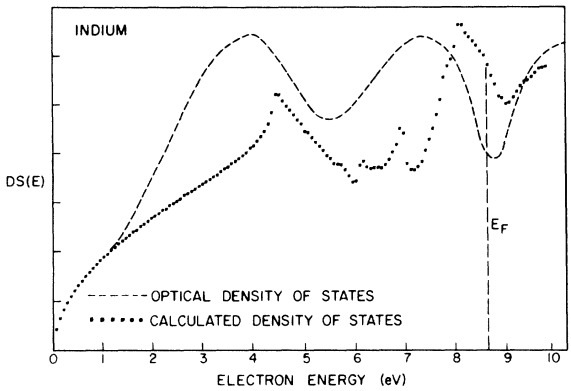

FIG. 7. Calculated density of states for indium (4-OPW), and the empirically determined optical density of states.

increment of energy surface at E. When the gradient becomes small, particularly at the zone boundaries, the density-of-states function develops singularities. The energy gaps at the zone faces change the local curvature of the bands and cause a departure from the free-electron density of states. The largest deviation for indium occurs between 4.0 and 6.0 eV. This is caused primarily by the large band gap at the L face (hexagonal face) of the Brillouin zone, and results in the peak near 4.5 eV and the valley at 6.0 eV. The structure near the Fermi energy is a result of the interaction of the band gaps at the x face and the z face of the zone. The small resolved peak near 7.0 eV is not seen in the results of Ref. 20 and 21, although the same band structure was used. This is primarily due to the approximations used in the present calculations which resulted in the mismatch of bands at the two interior faces of the pseudo $\frac{1}{48}$ sectors.

Figure 8 shows the calculated electron energy distributions for indium using direct transitions with broadening. In each box, the upper histogram represents the internal distribution of photoexcited electrons; the lower represents the external EDC. The external spectrum was calculated by applying the appropriate threshold function to the internal distribution.[1] Broadening has been introduced into these curves by allowing a finite spread in the excitation spectrum (0.3 eV). Although the EDC (lower curves) are normalized with respect to each other, no attempt was made to scale them to the absolute yield. In general, all of the EDC display a rather strong valley separating a leading doublet peak from a low-energy peak. The correspondence of the structure in the EDC with similar structure in the density of states (Fig. 7) is evident. An important feature to note is the behavior of this structure as a function of the photon energy. Similar to the experimental energy distributions of Fig. 3, the structures in the calculated EDC move with increments in the final-state energy equal to the increments in the photon energy; plotted with respect to the initial states, these features would remain at a fixed energy; this is seen in Fig. 9 and can be compared with the experimental distributions of Fig. 4. As it was seen in earlier results from aluminum,[1] copper,[16] and palladium,[17] it is found here that some features which are characteristic of nondirect transitions can also be seen as a result of direct transitions. Despite the 0.3-eV broadening introduced into the calculated EDC, there are detailed differences between them and the experimental EDC. For example, experimental EDC have only a single broad peak near the maximum energy whereas two narrower peaks appear in the calculated EDC. Another difference is that width and relative amplitude of the peaks in the calculated EDC vary with $\hbar\omega$ much more than the experimental results.

Another feature that is seen in the calculated EDC of Fig. 8 is the apparent band width due to the photoemitted electrons. At a photon energy of 12.8 eV, the lowest excited electron has sufficient energy to escape. However, these low-energy electrons did not come from the Γ point at the bottom of the band. Excitation of electrons from Γ would require much higher photon energies ($\hbar\omega \sim 20$ eV). Thus, the full bandwidth of 8.6 eV would not be evident until such photon energies are incident. In the case of nondirect transitions (Sec. IV C), the full bandwidth would be accessible when the photon energy exceeded the bandwidth plus the work function (~ 12.6 eV). This is just beyond the reach in the present experiment due to the cutoff of the LiF window.

C. EDC Calculated on Basis of Nondirect Transitions

In earlier studies of photoemission and the electronic structure of solids, Spicer[22] and Berglund and Spicer[2] suggested the nondirect transition to account for an apparent lack of importance to conserve $\vec{k}$. Based on their observations, they proposed a model in which (i) conservation of $\vec{k}$ is unimportant as a selection rule and (ii) that the optical-transition probability is proportional to a product of initial and final density-of-states factors. In 1967, Spicer[14] reviewed the available experimental data and made qualitative suggestions as to possible reasons for the nondirect transitions. Doniach[15] has recently presented many-body calculations which give some support to the nondirect picture. In the considerations of both Spicer and Doniach, nondirect transitions were expected from high-mass relatively tightly bound states, such as the d states of metals, rather than from almost free-electron states as in indium. However, the present authors[21] found previously that the experimental data from indium can qualitatively be de-

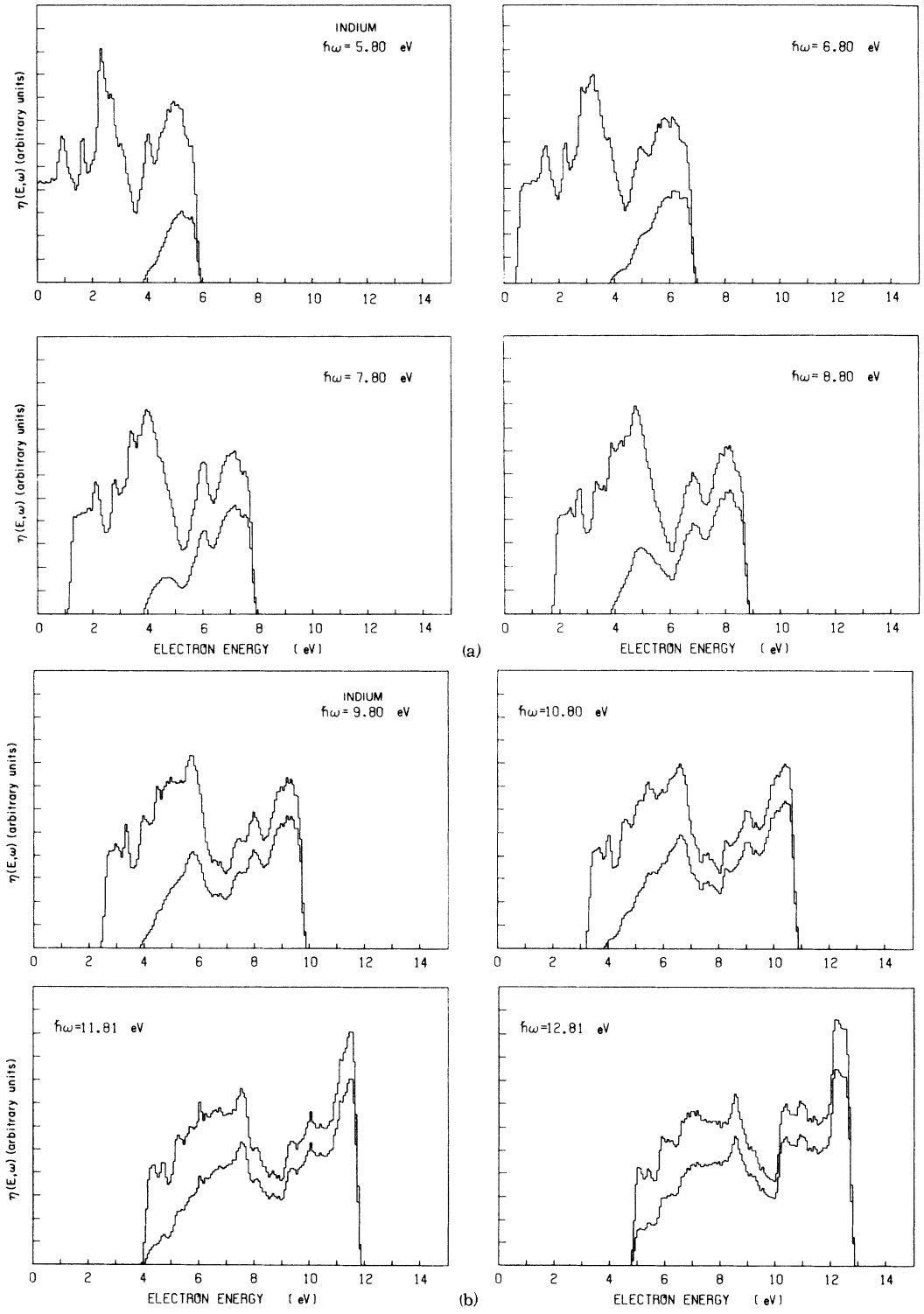

FIG. 8. (a) and (b) Calculated EDC for indium assuming direct transitions.

scribed by a convolution of density-of-states factors. Therefore, in order to make a comparison of results with the direct-transition model, the nondirect model will be discussed here.

The nondirect model assumes that the energy distribution of emitted electrons takes the form

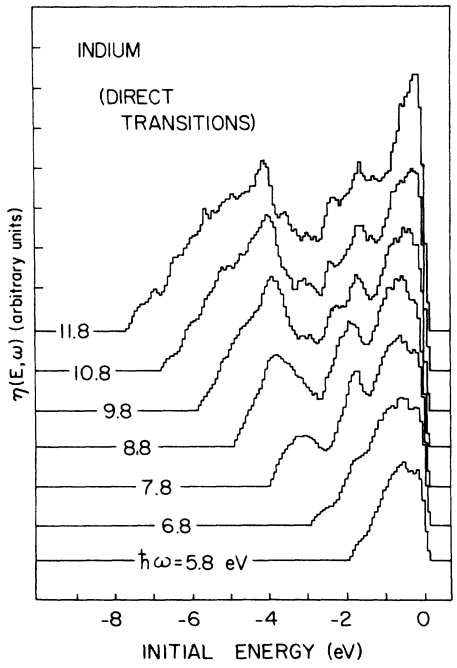

FIG. 9. Calculated direct transition EDC plotted with respect to the initial states.

$$N(E, \omega) = A\, C[\alpha(\omega),\ L(E),\ T(E)]N(E)N(E - \hbar\omega), \tag{4}$$

where $N(E - \hbar\omega)$ and $N(E)$ are, respectively, the initial- and final-states densities. $\alpha(\omega)$ is the optical-absorption coefficient, $L(E)$ is the characteristic length which determines the probability that an excited electron will reach the surface, and $T(E)$ is the probability of escape for an electron. The function C can be called an over-all escape factor, and A is a normalizing constant. Further details are given in Ref. 5 and we essentially follow the technique described in Ref. 23.

The method is empirical in that the density of final states $N(E)$ and initial states $N(E - \hbar\omega)$, which gives the best over-all fit to the experiment, are determined iteratively. The result of such an analysis is called an "optical density of states" (ODS). For indium, we assumed a bandwidth of 8.6 eV (corresponding to the free-electron width) and a work function of 4.0 eV; the results are shown in Fig. 7 and compared to the derived band density of states. There are some gross similarities, but the empirical ODS obviously does not reflect the details of the singularities of the calculated density of states. This is to be expected since the ODS reflects the experimental data which does not have any sharp features.

Figures 10 and 11 show the EDC and yield determined from the empirical ODS of Fig. 7. In the calculation of the yield, the energy-dependent electron-scattering length $L(E)$ was adjusted by a multiplicative constant over a range to find the best fit to the experimental values. Shown in Fig. 11 are yield curves with the scattering length equal to 50, 200, and 1600 Å at an energy 8.5 eV above the Fermi energy. The lowest curve [$L(8.5) = 50$ Å] gives a reasonable fit to experiment up to about 7.5 eV; at this point, the experimental data make a sharp increase. The curve for $L(8.5) = 1600$ Å fails to fit the yield at either the high or the low energies; undoubtedly, 1600 Å is an unreasonably long

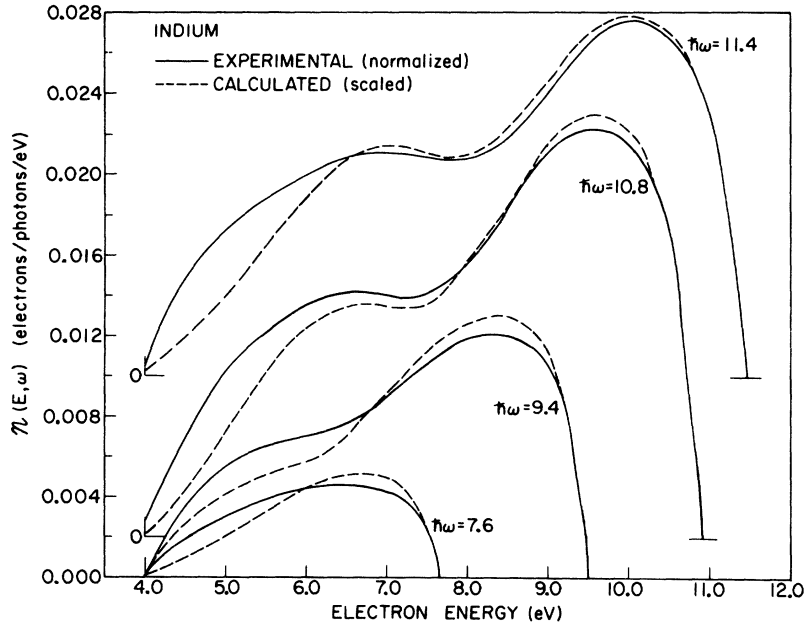

FIG. 10. Experimental EDC compared to the EDC calculated from the deduced optical density of states (the calculated yields have been adjusted to the experimental data).

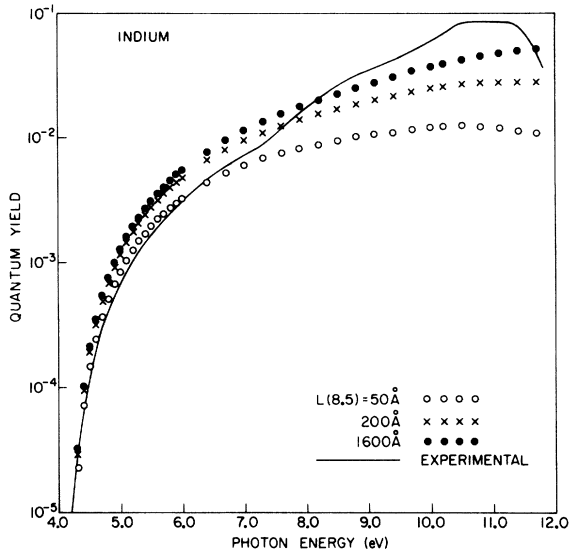

FIG. 11. Experimental yield of the crystalline sample compared to the yield calculated from the nondirect model using various electron-electron mean free paths.

scattering length. It is evident that an exact prediction of the yield is not possible. Although the absolute yield is quite sensitive to the scattering length, the over-all shape of the EDC is not. In Fig. 10, the shape of the EDC was calculated on the basis of $L(8.5) = 200$ Å; the absolute magnitudes were adjusted to match the experimental yields. The nondirect analysis is successful in predicting the shape of the experimental spectrum over a large photon energy range, but does not give good results for the absolute yield.

Recent work by Endriz and Spicer[3] on aluminum has indicated that (i) surface plasmons may be optically excited by surface roughness, and (ii) that the surface plasmon has a high probability of decaying with the excitation of a photoelectron. In aluminum, the surface-induced plasmon causes significant enhancement of the photoyield between 8.0 and 11.0 eV ($\hbar\omega/\sqrt{2} = 10.4$ eV). For indium, the "free-electron" surface plasmon occurs at $\hbar\omega/\sqrt{2} = 8.7$ eV. Energy-loss measurements by Robbins[24] indicate a loss peak near 8.7 eV which can be attributed to the surface loss. It is possible that some of the discrepancy between the experimental and the calculated yields of Fig. 11 [particularly for the case $L(8.5) = 50$ Å] can be attributed to a surface plasmon contribution to the experimental yield; this onset is near 7.5 eV and of course is not accounted for in the nondirect calculation. In fact, such an effect could also account for the large difference in yield between the crystal and liquid sample (Fig. 6) since the liquid should not have surface roughness and thus no coupling to surface plasmons would be possible. We could expect, however, that the largest enhancement due to surface plasmons would occur near 8.7 eV. The divergence of the two yield curves of Fig. 6 continues beyond 10 eV suggesting that another mechanism dominates the crystal yield at high photon energies.

Figure 12 compares the experimental EDC to the two calculated EDC's for a photon energy of 10.8 eV. The absolute magnitudes of the curves have been adjusted for the sake of comparison. It is evident that the nondirect-transition calculation gives reasonable agreement with experiment; this is to be expected since the ODS, from which this EDC was calculated, was determined from experiment. There is less agreement for the direct-transition calculation. However, the gross trend indicates the presence of at least two major groups of electrons. The lack of more detailed agreement can probably be traced to a number of sources. The most obvious would be the band-structure calculation of the energies. Although the potentials were adjusted for a best fit to Fermi-surface data,[20] this would not necessarily guarantee accurate eigenvalues away from the Fermi energy. Some contribution to the discrepancy can be traced to the approximations introduced by the division of the $\frac{1}{16}$ sector into the three inequivalent "$\frac{1}{48}$" zones and using the 4-OPW calculation instead of the 6-OPW. Aside from the calculation, another distinct source of error could be the experimental data itself. Strong inelastic scattering in the emission process would tend to wash out details of the experimental EDC, particularly at the high-energy end. This could introduce an uncertainty in $\vec{k}$ and move the optical selection rules toward those of the nondirect model. At any rate, we do not present a case for detailed agreement here. The calculations show that either model can give a qualitative description of the photoemission process in indium. However, from a simple theoretical stand-

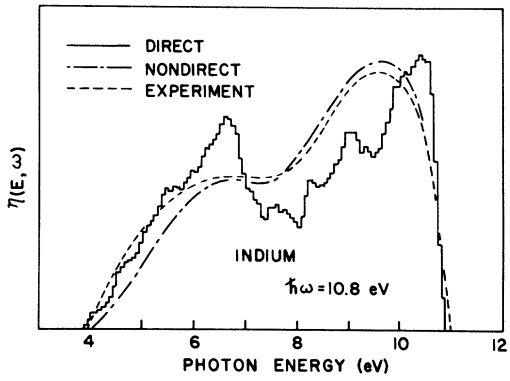

FIG. 12. Comparison of the experimental EDC to the calculated EDC's using the direct and nondirect models at a photon energy of 10.8 eV.

point, the known free-electron nature of indium would favor the direct-transition model.

V. DISCUSSION OF RESULTS FROM LIQUID INDIUM

During the past decade, a significant quantity of theoretical and experimental work considering the electrical properties and electronic structure of liquid metals has been presented. A number of theoretical papers consider the conductivity problem as well as the electronic structure.[25-27] The approach to the band-structure problem ranges from the free-electron theory of Ziman[26] to the "pseudobands" of Knight *et al.*[27] The available experimental data on liquid metals include measurements of x-ray diffraction,[28,29] optical properties,[12,30,31] characteristic energy losses,[32-34] and x-ray emission.[35,36]

Let us examine the systematics of the results from the last three types of experiments, i.e., those involving strong electronic excitations. These results can be classified according to whether or not the transitions or excitation observed disappear when the long-range order is destroyed by melting. The optical structure studied can be divided into two classes: (i) the direct transitions between states which would be free-electron-like, except for the periodic potential, and (ii) transitions from d states (or f states) which would not be free-electron-like even in the absence of a periodic potential. Two examples of each case are contained in the references quoted above. The transitions near 1.5 eV in Al[31] and Hg[12] are clearly of the first type; these transitions disappear when the crystalline samples are melted. Similar behavior is seen in the 1.5-eV transitions for solid indium[4] and liquid indium.[30(a)] In contrast to this behavior, the optical-absorption edge due to Fermi-level transitions of d-band electrons in Cu and Ag[31] does not disappear on melting, although some of its sharpness is lost. In addition, recent measurements of photoemission from liquid Au[37] verify the persistence of d-band structure in the liquid.

Soft-x-ray emission measurements of the L_{23} level of aluminum by Caterall and Trotter[36] indicate that the emission spectrum for the liquid differs very little from that of the crystalline solid. Powell[34] has measured the electron energy-loss spectra for liquid aluminum as well as for the solid. He found that both the surface and bulk plasmons could be identified for a range of temperature right through the melting point. A discontinuity at the melting point was consistent with the known change in the mass density of aluminum at the melting point. In the same paper, he also described the results for Bi, Au, In, Ga, and Hg and found, in general, that the loss spectra for these liquid metals were quite similar to those for the corresponding solid. One can summarize these results in the following way: Electronic excitations must involve states which are a direct and unique consequence of the long-range order if they are to disappear when melting destroys the long-range order.

To first order, the electron-energy distributions of Fig. 5 show the same leading peak that the crystalline solid shows (Fig. 3). A discussion of the origin of such structure was given in Sec. IV B. If the structure of Fig. 3 can be attributed to the density of states, then one could conclude that the structure of Fig. 5 (particularly the leading peak and the valley that follows it) has the same density-of-states origin. This strongly suggests that the density of states of indium changes very little on melting. From an intuitive point of view, one could consider that, although the long-range order is destroyed, the local coordination changes very little. In this respect, it is of interest to note that the measurements of Ocken and Wagner[29] indicate a change in coordination number from 10.5 to 10.1 atoms on heating liquid indium from 170 to 280 °C. In addition, their measurements reveal that the interatomic distance changes on the order of 0.06 Å (decreasing) with a 500 °C increase in temperature. Such small changes of short-range order may have only moderate effect on the electronic structure. Thus, as suggested by Knight *et al.*,[27] the energy structure of such metals may be more a consequence of local order than of long-range order.

Judging by the behavior of Al and Hg, one would expect the characteristic optical direct transition near a photon energy of 1.5 eV to disappear on melting. Theoretically, that is reasonable since that transition depends on $\vec{k}$ conservation and, thus, Bragg reflection and long-range order. In contrast, the present results seem to indicate that gross features of the density of states, even in an almost free-electron metal such as In, do not depend on long-range order but can be related to the short-range order which persists into the liquid. Thus, it would be very interesting to use photoemission as well as other methods to look at the density of states in liquid Al and Hg as well as In. The techniques used by Eastman on Au might be applicable to Al.

Shaw and Smith[38] have used a perturbation technique with a model potential to calculate the density of states for both the crystalline and liquid phases of indium. Their results for the crystal show structure similar to that shown in the calculated curve of Fig. 7, but on a considerably smaller scale. For the liquid, their results show virtually no structure although the over-all shape seems to follow the trend of the crystal density of states. The net result is that the liquid density of states is a highly smoothed crystal density of states. This general behavior may be consistent with the results from

this experiment; however, the magnitude of their predicted deviation from the free-electron density of states is so much smaller than the observed experimental structure and the experimental results are sufficiently obscured by scattering effects that it is difficult to make a definitive comparison.

VI. SUMMARY

Measurements of the photoemission energy distributions from crystalline indium reveal two major groups of electrons. These electron excitations (whether direct or nondirect) can be traced to corresponding features in the density of occupied states; major structure is due to the large band gap at the L face of the Brillouin zone. Similar structure is observed in the measurements from liquid-phase indium. This suggests that only small changes occur in the valence density of states on melting. Since only short-range order is retained in the liquid, it would appear that potentials giving rise to structure in the occupied states is more a consequence of short-range order than long-range order.

Calculation of energy distributions based on two different excitation mechanisms was made. Although neither mechanism can explain fully the quantitative features of the experiment, either can give a qualitative description. A "natural" consequence of the nondirect model is to give an optical density of states which resembles the experimental distributions. By contrast, there is no *a priori* reason to expect direct transition EDC to resemble the density of states. However, as it was found earlier for aluminum, the calculated direct transition EDC show a strong resemblance to the calculated density of filled states. This feature of both calculations supports the contention that observed structure in the experimental EDC is due to structure in the occupied density of states.

---

†Supported by U.S. Army Contract No. DA 44-009 AMC-1474(T), Center for Materials Research Contract No. SD-87, and the Joint Services Contract No. N00014-67-A-0112-0044.

*Present address: National Bureau of Standards (SURF-Syachrotron Ultraviolet Radiation Facility), Washington, D.C. 20234.

[1]R. Y. Koyama and N. V. Smith, Phys. Rev. B 2, 3049 (1970).

[2]C. N. Berglund and W. E. Spicer, Phys. Rev. 136, A1030 (1964); 136, A1044 (1964).

[3]J. G. Endriz and W. E. Spicer, Phys. Rev. Letters 24, 64 (1970); and unpublished.

[4]R. Y. Koyama and W. E. Spicer (unpublished).

[5]R. Y. Koyama, Ph.D. thesis (Stanford University, 1969) (unpublished).

[6]W. E. Spicer and C. N. Berglund, Rev. Sci. Instr. 35, 1665 (1964); and R. C. Eden, *ibid.* 41, 242 (1970).

[7]The high-vacuum chamber was designed by R. J. Powell [Ph.D. thesis (Stanford University, 1967) (unpublished)].

[8]The authors are indebted to G. Martin of the Center for Materials Research at Stanford University for making the x-ray diffraction measurements.

[9]W. E. Spicer, in *Photoelectric Emission in Optical Properties of Solids*, edited by F. Abelès (North-Holland, Amsterdam, to be published).

[10]A. T. Fromhold, Jr., Nuovo Cimento 28, 1127 (1963).

[11]The pumping system is described by R. C. Eden, Ph.D. thesis (Stanford University, 1967) (unpublished).

[12]E. G. Wilson and S. A. Rice, Phys. Rev. 145, 55 (1966).

[13]J. van Laar and J. J. Scheer, Philips Res. Rept. 15, 1 (1960).

[14]W. E. Spicer, Phys. Rev. 154, 385 (1967).

[15]S. Doniach, Phys. Rev. B 2, 3898 (1970).

[16]N. V. Smith and W. E. Spicer, Opt. Commun. 1, 157 (1969); and N. V. Smith, Phys. Rev. (to be published).

[17]J. F. Janak, D. E. Eastman, and A. R. Williams, Solid State Commun. 8, 271 (1970).

[18]D. T. Pierce and W. E. Spicer, Phys. Rev. Letters 25, 581 (1970).

[19]F. Wooten, T. Huen, and R. N. Stuart, in *Optical Properties and Electronic Structure of Metals and Alloys*, edited by F. Abelès (North-Holland, Amsterdam, 1966), p. 333.

[20]N. W. Ashcroft and W. E. Lawrence, Phys. Rev. 175, 938 (1968).

[21]R. Y. Koyama, W. E. Spicer, N. W. Ashcroft, and W. E. Lawrence, Phys. Rev. Letters 19, 1284 (1967).

[22]W. E. Spicer, Phys. Rev. Letters 11, 243 (1963).

[23]W. F. Krolikowski and W. E. Spicer, Phys. Rev. 185, 882 (1969).

[24]J. L. Robbins, Proc. Phys. Soc. (London) 79, 119 (1962).

[25]L. E. Ballentine, Can. J. Phys. 44, 2533 (1969); B. L. Gyorffy, Phys. Rev. B 1, 3290 (1970); P. Phariseau and J. M. Ziman, Phil. Mag. 8, 1487 (1963); T. E. Faber and J. M. Ziman, *ibid.* 11, 153 (1965); C. C. Bradley, T. E. Faber, E. G. Wilson, and J. M. Ziman, *ibid.* 7, 865 (1962); S. F. Edwards, Proc. Roy. Soc. (London) A267, 518 (1962); N. V. Smith, Phys. Rev. 163, 552 (1967); and Phys. Letters 26A, 126 (1968).

[26]J. M. Ziman, Phil. Mag. 6, 1013 (1961).

[27]W. D. Knight, A. G. Berger, and V. Heine, Ann. Phys. (N.Y.) 8, 173 (1959).

[28]C. Gamertsfelder, J. Chem. Phys. 9, 450 (1941).

[29]H. Ocken and C.N.J. Wagner, Phys. Rev. 149, 122 (1966).

[30](a) J. N. Hodgson, Phil. Mag. 7, 229 (1962); (b) L. G. Schulz, J. Opt. Soc. Am. 47, 64 (1957).

[31]J. C. Miller, Phil. Mag. 20, 1115 (1969).

[32]H. Boersch, J. Geiger, H. Hellwid, and H. Michel, Z. Physik 169, 252 (1962).

[33]C. J. Powell, Phys. Rev. Letters 15, 852 (1965); Advan. Phys. 16, 203 (1967).

[34]C. J. Powell, Phys. Rev. 175, 972 (1965).

[35]D. W. Fisher and W. L. Baun, Phys. Rev. 138, A1047 (1965).

[36]J. A. Caterall and J. Trotter, Phil. Mag. 8, 897 (1963).

[37]D. E. Eastman, Phys. Rev. Letters 26, 1108 (1971).

[38]R. W. Shaw and N. V. Smith, Phys. Rev. 178, 985 (1969).